J. Fluid Mech. (1989), *vol.* 202, *pp.* 17–41
Printed in Great Britain

A study of linearized oscillatory flow past particles by the boundary-integral method

By C. POZRIKIDIS

Department of Applied Mechanics and Engineering Sciences, R-011, University of California at San Diego, La Jolla, CA 92093, USA

(Received 15 January 1988 and in revised form 26 September 1988)

Viscous oscillatory flow past particles, governed by the unsteady Stokes equation, is considered. The problem is addressed in its general form for arbitrary flows and particle shapes using the boundary-integral method. It is shown that the leading-order correction to the force exerted on a particle in unsteady flow may be inferred directly from the drag in steady translational motion. For axisymmetric flow, a numerical procedure for solving the boundary-integral equation is developed, and is applied to study streaming oscillatory flow past spheroids, dumbbells, and biconcave disks. The effect of the particle geometry on the structure of the flow is studied by comparing the streamline pattern associated with these particles to that for the sphere. The results reveal the existence of travelling stagnation points on the surface of non-spherical particles, and the formation of unsteady viscous eddies in the interior of the flow. These eddies grow during the decelerating flow period, and shrink during the accelerating flow period. For particles with concave boundaries, unsteady free eddies may originate from an expansion of wall eddies that reside within the concave regions.

1. Introduction

Oscillatory flows are of interest in several fields of engineering and science, most notably in the areas of aeroacoustics, chemical engineering, and biomechanics. There is a rich phenomenology associated with these flows that has prompted a number of experimental and theoretical investigations.

In general, previous work may be classified in two categories that address internal and external flows respectively. Typical in the first category are studies of oscillatory flow within furrowed and indented channels (Hall 1974; Sobey 1980, 1982, 1983, 1985*a*, *b*; Ralph 1986), flow over square cavities (Ghaddar *et al.* 1986), and flow within collapsible tubes with oscillating cross-section or with oscillating indentations (Pedley & Stephanoff 1985; Padmanabhan & Pedley 1987). Topics of interest include the analysis of steady streaming motion, the description of the flow kinematics as a function of the Strouhal and the Reynolds number, the study of particle convection, fluid dispersion, and convective scalar transport, and the analysis of hydrodynamic instabilities triggered by flow oscillations. The second category includes studies of flow past isolated particles and drops (or in general, finite bodies) or collections of them, with typical applications in the fields of acoustics and suspension mechanics (Riley 1967; Pienkowska 1984). An important objective of the analysis is the computation of the force and the torque acting on the particles, as well as the derivation of equations describing the motion of the particles (Clift, Grace & Weber 1978, ch. 11).

One of the most remarkable features of viscous oscillatory flow is its ability to enhance convective transport and fluid mixing while maintaining a laminar environment (Sobey 1985*b*). This is attributed to a rather complicated kinematics involving the generation and subsequent expansion of viscous eddies in the vicinity of curved boundaries. This feature offers opportunities for novel engineering design in processes involving sensitive materials such as chemical emulsions and blood.

In the present paper we are concerned with external oscillatory flow past particles. At the outset, we would like to state the basic premise of our analysis, which is that the frequency parameter of the flow, defined as $\beta = \omega d^2/\nu$, is larger than the Reynolds number, $Re = Ud/\nu$ (ω is the angular velocity, d is the characteristic size of the particle, and U is a peak velocity in the flow). More precisely, we require that $\beta > cRe$, where c is a constant dependent on the geometry of the flow. Furthermore, since β is equal to the product of the Reynolds to the Strouhal (St) number, $\beta > cRe$ implies that $St = \omega d/U > c$. Straightforward scaling of the equation of motion shows that this assumption allows linearization of the equation of motion, with considerable simplifications in the analytical and computational procedures (Happel & Brenner 1973, §2.10). Physically, linearization requires that the maximum excursion of fluid particles, over one period of the flow, is small compared to the characteristic size of the particles (Batchelor 1967). In this fashion, the Lagrangian time derivative in the equation of motion may be accurately approximated by the Eulerian time derivative. Furthermore, linearization allows us to infer general time-dependent flow from its harmonic components through the use of integral transforms (Basset 1888; Lawrence & Weinbaum 1986). For instance, the instantaneous force on a particle in general time-dependent motion may be deduced from that in oscillatory motion. Examples of physical situations where linearization is valid include Brownian motion, and the unsteady interaction of particles settling at low Reynolds numbers. A numerical demonstration of the validity of linearization at high Strouhal numbers (and at finite Reynolds numbers) was given by Sobey (1980, §4.4).

Linearized viscous flow exhibits unique kinematic characteristics. At low frequencies, it reduces to steady (or more precisely, quasi-steady) Stokes flow with diffuse vorticity. At high frequencies, it reduces to potential flow everywhere, except within thin boundary layers of thickness $(\nu/\omega)^{\frac{1}{2}}$ residing along the solid boundaries of the flow. If the flow has a mean component, these oscillatory boundary layers, called Stokes layers, may coexist with Prandtl type boundary layers at high Reynolds numbers. Linearized unsteady viscous flow is reversible. This implies that there may not be a lifting force on a particle accelerating in a symmetric flow domain, for instance on a sphere accelerating above and parallel to a plane wall. This may be contrasted to the case of inviscid potential flow. Furthermore, linearization prevents the onset of inertial, steady streaming flow. This may be considered as a nonlinear, finite Reynolds number effect on the basic linear flow, and may be treated as such from an analytical or computational perspective.

Previous work on linearized viscous flow past isolated particles may be traced back to the seminal work of Stokes (1851) who studied flow due to longitudinal oscillations of a sphere or a cylinder. A number of subsequent authors have addressed flow due to oscillations of spheroids and disks. More specifically, the spheroidal shape was considered by Buchanan (1891), Kanwal (1955), Lai & Mockros (1972), and Lawrence & Weinbaum (1986, 1988). Unsteady particle interactions have also been studied both in the context of the unsteady Stokes' equation (Pienkowska 1984) and of the mathematically equivalent Brinkman's equation (Kim & Russel 1985). In addition, certain general theorems pertaining to linearized motion have been

established. These include the reciprocal relationship, the boundary-integral formulation, and Faxen's laws. A more detailed review of the literature and further references may be found in the recent articles by Lawrence & Weinbaum (1988), and Pozrikidis (1988*b*).

In this paper we seek to obtain further insights into the physics of unsteady viscous flow through numerical solutions of the unsteady Stokes equation. One of our main objectives will be to analyse the effect of boundary geometry on the structure of the flow, with special emphasis on unsteady flow reversal. To this end we note that whereas steady flow reversal has been studied rather extensively by computational and analytical means (Hasimoto & Sano 1980), unsteady flow reversal has received relatively little attention (Bentwich & Miloh 1978; Smith 1987). In our computations we will consider two families of particle shapes including spheroids, and particles in the form of biconcave disks and dumbbells. The former will allow us to study the effect of particle aspect ratio, and the latter will allow us to examine the effect of concave boundaries on the structure of the flow.

From the point of view of computational fluid dynamics, our work was triggered by the success of certain recent numerical methods in the area of low-Reynolds-number hydrodynamics. These include the singularity method (Chwang & Wu 1975; Dabros 1985; Kim 1986), the method of multipole expansions (Gluckman, Pfeffer & Weinbaum 1971), and the boundary-integral method and its variations (Pozrikidis 1988*a*). These methods have proven to be invaluable in the study of various exterior, interior, steady and quasi-steady creeping flows, in two-dimensional, axisymmetric, and three-dimensional geometry, including problems with free surfaces and fluid interfaces. The unsteady Stokes equation (as well as the related Brinkman's equation) is mathematically similar to the steady Stokes equation, in the sense that it constitutes a linear, elliptic, boundary-value problem. Thus, the above methods have their counterpart for unsteady flow, and their implementation provides us with new techniques for tackling fundamental problems of longstanding interest.

Kim & Russel (1985) adopted the method of reflections and the method of multipole expansions to study the interaction of two spheres in Brinkman's medium. Pozrikidis (1988*b*) considered the singularity method for unsteady linearized flow, and addressed a set of fundamental problems involving axisymmetric particles. Although in principle the singularity method may be formulated for general three-dimensional flows and arbitrary shapes, in practice, it is most efficient for slender particles or for particles with relatively simple, convex boundaries. In this article we address the boundary-integral method for oscillatory linearized flow. Briefly, in this method, the velocity field is expressed as an integral of the velocity, stress, or in general, of singularity densities along the boundary of the flow, and the solution to the problem is reduced to the calculation of the boundary distributions. In turn, this requires the solution of Fredholm integral equations of the first or second kind. Effectively, the dimension of the mathematical problem is reduced with respect to that of the physical problem by one, resulting in considerable simplifications. One of the basic strengths of the boundary integral method is that it may be readily implemented for concave or irregular boundaries, and for arbitrary ambient flows. The origin of the boundary integral method for unsteady linearized motion may be traced back to the work of Oseen (1927). Its precise formulation for oscillatory flow is due to Williams (1986).

In §2 we present a short derivation of the boundary-integral formulation. Although in our derivation we consider infinite external flow past particles, we indicate that the method has a much more general applicability, and may be readily

adapted to describe internal, semi-infinite, or bounded flows. Next, we consider the asymptotic behaviour of the integral equation at large and small frequencies, and outline a formal way of obtaining asymptotic results for the total force acting on a particle. It is in the merit of the boundary-integral formulation that these results are obtained with very little analytical effort, and in a compact form. In §3 we consider the numerical solution of the integral equation for axial streaming flow past axisymmetric particles, or equivalently, for flow produced by longitudinal oscillations of axisymmetric particles. In §4 we present numerical results for spheroids, biconcave disks, and dumbbells. We conclude the paper in §5 with closing remarks.

2. Formulation

We consider oscillatory flow past a single particle, or a finite collection of particles, governed by the unsteady Stokes' equation. We assume that the flow is infinite in extent in all directions. Thus, we write for the velocity and the pressure $\boldsymbol{U} = \boldsymbol{u}\exp(-\mathrm{i}\omega t)$ and $P = p\exp(-\mathrm{i}\omega t)$, and substitute into the linearized equation of motion to obtain a Helmholtz-type equation. In dimensionless form this reads

$$\lambda^2 \boldsymbol{u} = -\nabla p + \nabla^2 \boldsymbol{u}. \tag{2.1}$$

The frequency parameter λ^2 is defined as $\lambda^2 = -\mathrm{i}\omega d^2/\nu$, where d is characteristic of the size of the particles and ν is the kinematic viscosity of the fluid. The continuity equation remains unaffected with respect to $\boldsymbol{u}$,

$$\nabla \cdot \boldsymbol{u} = 0. \tag{2.2}$$

Noting that (2.1) is a linear elliptic equation suggests that its solution may be expressed as an integral along the boundaries of the flow. To develop the boundary integral formulation, we follow the well-established theory for steady Stokes flow (Ladyzhenskaya 1969), and write the reciprocal relationship

$$\operatorname{div}(u_i^* \sigma_{ik} - u_i \sigma_{ik}^*) = 0, \tag{2.3}$$

$\boldsymbol{u}^*$ and $\boldsymbol{u}$ are arbitrary non-singular solutions to the system (2.1), (2.2), with corresponding stress fields $\boldsymbol{\sigma}^*$ and $\boldsymbol{\sigma}$. We now adopt the oscillating Stokeslet, centred on an arbitrary point $\boldsymbol{x}_0$, as our solution for $\boldsymbol{u}^*$ (Williams 1966). Thus, reverting to dimensional variables we set

$$u_i^* = \frac{1}{8\pi\mu} S_{ij}(\hat{\boldsymbol{x}})\, a_j, \tag{2.4a}$$

$$\sigma_{ik}^* = \frac{1}{8\pi} T_{ijk}(\hat{\boldsymbol{x}})\, a_j, \tag{2.4b}$$

where $\hat{\boldsymbol{x}} = \boldsymbol{x} - \boldsymbol{x}_0$, and $\boldsymbol{a}$ is an arbitrary constant expressing an oscillatory point force. The tensor $\boldsymbol{S}(\boldsymbol{x}, \lambda)$ is given by

$$S_{ij} = \frac{\delta_{ij}}{r} A + \frac{\hat{x}_i \hat{x}_j}{r^3} B, \tag{2.5}$$

where $r = |\hat{\boldsymbol{x}}|$, and the functions A and B are defined as

$$A = 2\,\mathrm{e}^{-R}\left(1 + \frac{1}{R} + \frac{1}{R^2}\right) - \frac{2}{R^2}, \tag{2.6a}$$

$$B = -2\,\mathrm{e}^{-R}\left(1 + \frac{3}{R} + \frac{3}{R^2}\right) + \frac{6}{R^2}, \tag{2.6b}$$

with $R = \lambda r$. As $R \to 0$, $A, B \to 1$, and $\boldsymbol{S}$ reduces to the Oseen tensor for steady Stokes flow. Furthermore, at very large R, $\boldsymbol{S}$ behaves like a potential dipole, suggesting that far away from the Stokeslet the flow tends to become irrotational. $\boldsymbol{T}$ is the stress tensor associated with the oscillating Stokeslet.

Returning to (2.3), we select a point $\boldsymbol{x}_0$ in the domain of the flow, and integrate this equation in a volume constricted by the particles, a very large spherical surface extending to infinity, and a very small spherical surface centred at the Stokeslet. We then use the divergence theorem to obtain an integral expression for the velocity at the point $\boldsymbol{x}_0$ in terms of single-layer and double-layer distributions. For points on the surface of a particle this expression takes the form

$$u_j(\boldsymbol{x}_0) = -\frac{1}{4\pi\mu}\int_{S_p} [f_i(\boldsymbol{x}) S_{ij}(\hat{\boldsymbol{x}}) - u_i(\boldsymbol{x}) T_{ijk}(\hat{\boldsymbol{x}})\, \hat{n}_k(\boldsymbol{x})]\, \mathrm{d}S, \tag{2.7}$$

where $\boldsymbol{f} = \boldsymbol{\sigma}\cdot\hat{\boldsymbol{n}}$. For points in the interior of the flow, the factor $4\pi\mu$ in the denominator must be replaced by $8\pi\mu$. The integration is over all particle surfaces, with $\hat{\boldsymbol{n}}$ being the unit normal vector pointing into the fluid. In the derivation of the above equation, we have assumed that the velocity vanishes at infinity at a sufficiently fast rate. If this is not true, the equation must be applied for an appropriately chosen disturbance flow that satisfies this restriction.

Equation (2.7) may be conveniently simplified by extending the flow into the interior of each particle. Let $\boldsymbol{u}'$ be the internal flow that agrees with the external flow on the surface of the particle, and $\boldsymbol{f}' = \boldsymbol{\sigma}'\cdot\hat{\boldsymbol{n}}$ be the corresponding surface traction on the interior surface of the particle. It is then easy to show that (2.7) may be written in terms of a surface distribution of Stokeslets,

$$u_j(\boldsymbol{x}_0) = -\frac{1}{8\pi\mu}\int_{S_p} f_i''(\boldsymbol{x})\, S_{ij}(\hat{\boldsymbol{x}})\, \mathrm{d}S, \tag{2.8}$$

where $\boldsymbol{f}'' = \boldsymbol{f} - \boldsymbol{f}'$. This equation applies uniformly in the interior of the flow and on the particle surface. Note that the Stokeslet density distribution $\boldsymbol{f}''$ is no longer identified necessarily with the surface traction on the particle, and hence, the gain in simplicity may be counterbalanced by a compromise in the physical picture. For certain simple flows, $\boldsymbol{u}'$ and $\boldsymbol{f}'$ may be found by simple inspection. For instance, for flow produced by the translational oscillation of a particle, the velocity on the surface of the particle is a constant equal to $\boldsymbol{v}$, and $\boldsymbol{u}' = \boldsymbol{v}, \boldsymbol{f}' = \lambda^2 \boldsymbol{v}\cdot\boldsymbol{x}\hat{\boldsymbol{n}}$. When $\boldsymbol{u}$ represents the disturbance flow due to the presence of a particle, $\boldsymbol{f}''$ is equal to total surface stress on the particle (Howells 1974).

For axisymmetric flow, one may perform the integration in the azimuthal direction, reducing the surface integral into a line integral along the contour of each particle in a meridional plane

$$u_\alpha(\boldsymbol{x}_0) = -\frac{1}{8\pi\mu}\int_{C_p} M_{\alpha\beta}(\boldsymbol{x}, \boldsymbol{x}_0) f_\beta''(\boldsymbol{x})\, \mathrm{d}l, \tag{2.9}$$

where values of the indices $(1, 2)$, indicate the (x, σ)-direction respectively. Note the change in the order of the indices from (2.8) to (2.9). The matrix $\boldsymbol{M}$ is defined as

$$\sigma\begin{pmatrix} A_{10} + \hat{x}^2 A_{30} & \hat{x}(\sigma B_{30} - \sigma_0 B_{31}) \\ \hat{x}(\sigma B_{31} - \sigma_0 B_{30}) & A_{11} + (\sigma^2 + \sigma_0^2) B_{31} - \sigma\sigma_0 (B_{30} + B_{32}) \end{pmatrix}, \tag{2.10}$$

where

$$A_{mn} = \int_0^{2\pi} \frac{\cos^n \phi}{r^m} A\, \mathrm{d}\phi, \tag{2.11}$$

and similarly for B_{mn}, with A and B defined in (2.6*a*, *b*).

Now, given the (total or disturbance) velocity on the particle surface, (2.8) becomes a Fredholm integral equation of the first kind for the unknown surface force $\boldsymbol{f}''$. The form of this equation is identical to that developed by Youngren & Acrivos (1975) for steady Stokes flow. The complex nature of its kernel discourages analytical treatment, and directs us to asymptotic and numerical solutions.

2.1. *Asymptotic solutions*

Before resorting to numerical solutions it is helpful to consider the asymptotic behaviour of the derived integral equation (2.8) for very high, and very low frequencies. This will allow us to derive certain useful results for the force exerted on a particle. For clarity, we address the single-particle case, but we note that the many-particle case may be treated in an entirely analogous manner.

To obtain the asymptotic behaviour of the force on a particle immersed in high-frequency flow, we substitute in place of $\boldsymbol{S}$ its asymptotic form as $R = \lambda r$ tends to infinity, to obtain

$$u_j = -\frac{1}{4\pi\mu\lambda^2}\int_S \left(-\frac{\delta_{ij}}{r^3}+3\frac{\hat{x}_i\hat{x}_j}{r^5}\right)f_i''\,\mathrm{d}A. \tag{2.12}$$

This expresses irrotational flow, $\boldsymbol{u} = \nabla\Phi$, where the velocity potential Φ is produced by a surface distribution of source-dipoles

$$\Phi = \frac{1}{4\pi\mu\lambda^2}\int_S \nabla\frac{1}{r}\cdot\boldsymbol{f}''\,\mathrm{d}A. \tag{2.13}$$

Consistent with our assumptions, this equation is valid outside the viscous boundary layer, of thickness $1/|\lambda|$, residing along the particle surface. Thus, the flow produced by (2.12) satisfies the non-penetration but not the no-slip condition on the particle surface. Identifying (2.13) with a source–dipole distribution, yields

$$\boldsymbol{f}'' = \mu\lambda^2\Phi''\boldsymbol{n}, \tag{2.14}$$

where Φ'' the density of the distribution.

For a particle which executes translational oscillations with velocity $\boldsymbol{V} = \boldsymbol{v}\exp(-\mathrm{i}\omega t)$, we may write $\Phi'' = \boldsymbol{\phi}''\cdot\boldsymbol{v}$, where $\boldsymbol{\phi}_i''$ is the dipole distribution associated with motion in the i-direction, to obtain $\boldsymbol{f} = \mu\lambda^2\boldsymbol{\phi}\cdot\boldsymbol{v}\hat{\boldsymbol{n}}$. Integration over the surface of the particle gives the total force exerted on the particle as

$$\boldsymbol{F} = -\mathrm{i}\omega\rho\boldsymbol{v}\cdot\boldsymbol{A}, \tag{2.15}$$

where $\boldsymbol{A}$ is the added-mass tensor, given by

$$\boldsymbol{A} = \int_{S_p}\boldsymbol{\phi}\hat{\boldsymbol{n}}\,\mathrm{d}A, \tag{2.16}$$

(Yih 1979, p. 103). Thus, we have established that as is the case for inviscid flow, the leading term of the force on the particle in high-frequency linear flow is simply that due to the added mass. Higher-order viscous correction terms may be obtained by considering correspondingly higher-order terms in the expansion of the integral equation. In particular, the first correction term, proportional to λ, may be obtained in an alternative fashion, by considering the viscous dissipation in the boundary layer around the surface of the particle, as discussed by Batchelor (1967, p. 357).

Let us now consider the low-frequency limit. We seek to determine the behaviour of the force on the particle as an asymptotic series with respect to the frequency

parameter λ. The (total or disturbance) velocity on the surface of the particle is equal to $\boldsymbol{v}(\boldsymbol{x}, \lambda)$ (not necessarily a constant), and is assumed to be given in the statement of the problem. Thus, we expand $\boldsymbol{v}$, $\boldsymbol{S}$ and $\boldsymbol{f}''$ in a Taylor series with respect to λ,

$$\boldsymbol{v} = \boldsymbol{v}^{(0)} + \lambda \boldsymbol{v}^{(1)} + \lambda^2 \boldsymbol{v}^{(2)} + \ldots, \tag{2.17}$$

$$\boldsymbol{S} = \boldsymbol{S}^{(0)} + \lambda \boldsymbol{S}^{(1)} + \lambda^2 \boldsymbol{S}^{(2)} + \ldots, \tag{2.18}$$

$$\boldsymbol{f}'' = \boldsymbol{f}''^{(0)} + \lambda \boldsymbol{f}''^{(1)} + \lambda^2 \boldsymbol{f}''^{(2)} + \ldots, \tag{2.19}$$

where

$$\left.\begin{aligned} S_{ij}^{(0)} &= \frac{\delta_{ij}}{r} + \frac{\hat{x}_i \hat{x}_j}{r^3}, \\ S_{ij}^{(1)} &= -\tfrac{4}{3}\delta_{ij}, \\ S_{ij}^{(2)} &= \tfrac{1}{4} r^2 \left(3\frac{\delta_{ij}}{r} - \frac{\hat{x}_i \hat{x}_j}{r^3} \right), \end{aligned}\right\} \tag{2.20}$$

and substitute into (2.8). Collecting coefficients of same powers in λ gives a series of integral equations, the first three of which read

$$\boldsymbol{v}^{(0)} = -\frac{1}{8\pi\mu} \int_{S_p} \boldsymbol{f}''^{(0)} \cdot \boldsymbol{S}^{(0)} \, \mathrm{d}A, \tag{2.21a}$$

$$\boldsymbol{v}^{(1)} - \frac{1}{6\pi\mu} \boldsymbol{F}^{(0)} = -\frac{1}{8\pi\mu} \int_{S_p} \boldsymbol{f}''^{(1)} \cdot \boldsymbol{S}^{(0)} \, \mathrm{d}A, \tag{2.21b}$$

$$\boldsymbol{v}^{(2)} - \frac{1}{6\pi\mu} \boldsymbol{F}^{(1)} + \frac{1}{8\pi\mu} \int_{S_p} \boldsymbol{f}''^{(0)} \cdot \boldsymbol{S}^{(2)} \, \mathrm{d}A = -\frac{1}{8\pi\mu} \int_{S_p} \boldsymbol{f}''^{(2)} \cdot \boldsymbol{S}^{(0)} \, \mathrm{d}A, \tag{2.21c}$$

where $\boldsymbol{F}''^{(n)} \equiv \int \boldsymbol{f}^{(n)} \, \mathrm{d}A$. The first-order problem (2.21*a*) describes steady Stokes flow. The second-order problem (2.21*b*) may be split into two parts. The first part describes steady Stokes flow with boundary velocity $\boldsymbol{v}^{(1)}$. The second part describes steady Stokes flow produced by the particle translating with velocity $-\boldsymbol{F}^{(0)}/6\pi\mu$. For this second contribution we may write

$$\boldsymbol{f}''^{(1)} = \frac{1}{6\pi} \boldsymbol{r} \cdot \boldsymbol{F}''^{(0)}, \tag{2.22a}$$

$$\boldsymbol{F}''^{(1)} = \frac{1}{6\pi} \boldsymbol{R} \cdot \boldsymbol{F}''^{(0)}, \tag{2.22b}$$

where the resistance tensors $\boldsymbol{r}$ and $\boldsymbol{R}$ produce the surface stress distribution and total force on the steadily translating particle. Similarly, the second-order problem (2.21*c*) may be split into three parts. The first part corresponds to steady Stokes flow with the velocity on the particle surface equal to $\boldsymbol{v}^{(2)}$. The second part corresponds to steady particle motion with velocity $-\boldsymbol{F}^{(1)}/6\pi\mu$. The third part lacks simple physical interpretation.

In particular, for an oscillating particle, the velocity on the surface of the particle is a constant equal to $\boldsymbol{v}$, independent of λ, and we find that $\boldsymbol{f}'' = \boldsymbol{f} - \lambda^2 \boldsymbol{v} \cdot \boldsymbol{x}\hat{\boldsymbol{n}}$. The above relationships then yield the total force on the particle as

$$\boldsymbol{F} = -\left(\boldsymbol{R} + \frac{\lambda}{6\pi} \boldsymbol{R} \cdot \boldsymbol{R} + \frac{\lambda^2}{(6\pi)^2} \boldsymbol{R} \cdot \boldsymbol{R} \cdot \boldsymbol{R} \right) \cdot \boldsymbol{v} + \lambda^2 V_{\mathrm{p}} \boldsymbol{v} + \lambda^2 \boldsymbol{F}^{(2b)} + O(\lambda^3), \tag{2.23}$$

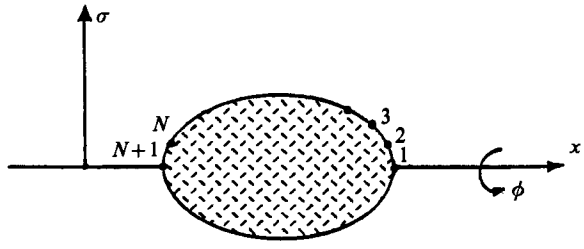

FIGURE 1. Definition sketch for an axisymmetric particle showing boundary discretization.

where V_p is the volume of the particle, and $\boldsymbol{F}^{(2b)} = \int \boldsymbol{f}^{(2b)}\,\mathrm{d}A$ must be found by solving the integral equation

$$\int_{S_p} \boldsymbol{f}''^{(0)}\cdot\boldsymbol{S}^{(2)}\,\mathrm{d}A = -\int_{S_p} \boldsymbol{f}''^{(2b)}\cdot\boldsymbol{S}^{(0)}\,\mathrm{d}A. \tag{2.24}$$

To first order, the surface stress distribution is given by

$$\boldsymbol{f} = -\left(\boldsymbol{r}+\lambda\frac{\mu}{6\pi}\boldsymbol{r}\cdot\boldsymbol{R}\right)\cdot\boldsymbol{v}+O(\lambda^2). \tag{2.25}$$

For an orthotropic particle, the resistance matrix $\boldsymbol{R}$ is diagonal, and the above equation states that to first order, the surface stress distribution is identical in functional form, with the steady distribution.

Perhaps the most important conclusion of the above asymptotic analysis is that the leading-order correction to the surface stress and to the force exerted on a particle which is impedded in general oscillatory flow may be found from the solution for steady translation. Higher-order corrections must be found by solving a series of boundary-value problems the first of which is described by the integral equation (2.21*c*). These results complement those of Kanwal (1964) and Williams (1966), for streaming axisymmetric, and streaming three-dimensional flow respectively.

3. Solution of the integral equation for axisymmetric flow

Our goal in this section is to develop a numerical procedure for solving (2.9) for $\boldsymbol{f}''$, given the boundary velocity $\boldsymbol{u}$. The steady version of this equation has been considered by several authors beginning with the pioneering investigation of Youngren & Acrivos (1975). Our approach is similar to that developed by previous authors, with certain important variations due to the complexity of our kernel. Below, we summarize our strategy, and comment on certain important issues of our numerical implementation.

As a first step, we represent the contour of the particle in a meridional plane using N elements that are defined by $N+1$ nodal points (figure 1), and approximate the surface stress over each element as a constant function $\boldsymbol{f}''_n$ ($n = 1,\ldots,N$). We then evaluate $\boldsymbol{f}''_n$ by applying the integral equation at the centre of each element $\boldsymbol{x}_m$ ($m = 1,\ldots,N$). In this fashion, we reduce the problem to solving a dense system of linear algebraic equations for $\boldsymbol{f}''_n$. Specifically, applying (2.9) at the collocation points yields a system of N equations

$$u(\boldsymbol{x}_m) = -\frac{1}{8\pi\mu}\sum_{n=1}^{N} \boldsymbol{I}_n(\boldsymbol{x}_m)\cdot\boldsymbol{f}_n, \tag{3.1}$$

where $m = 1, 2, \ldots, N$, and

$$\boldsymbol{I}_n(\boldsymbol{x}_m) = \int_{S_n} \boldsymbol{M}(\boldsymbol{x}_m)\, \mathrm{d}l. \tag{3.2}$$

S_n denotes integration over the nth element. After decomposing the radial and axial components of the above equations into their real and imaginary parts, we end up with a linear system of real equations of size $4N \times 4N$.

For the accurate evaluation of the singular integrals in (3.2), we write

$$\boldsymbol{I}_n(\boldsymbol{x}_m) = \int_{S_n} [\boldsymbol{M}(\boldsymbol{x}_m;\lambda) - \boldsymbol{M}(\boldsymbol{x}_m;0)]\, \mathrm{d}l + \int_{S_n} [\boldsymbol{M}(\boldsymbol{x}_m;0) + 2\ln(r)\boldsymbol{I}]\, \mathrm{d}l - 2\boldsymbol{I}\int_{S_n} \ln(r)\, \mathrm{d}l, \tag{3.3}$$

where $\boldsymbol{I}$ is the identity matrix. The kernel $\boldsymbol{M}(\boldsymbol{x}, 0)$ is provided by Youngren & Acrivos (1975), but for completeness, it is also given in Appendix A. The first two integrals on the right-hand side of the above equation are regular, and may be evaluated with sufficient accuracy by using a six- or twelve-point Gauss–Legendre quadrature. The third integral is singular, but it may be evaluated either analytically or numerically (by subtracting-off the singularity) over simple elements such as straight lines, parabolas, and circular arcs.

The integrand $\boldsymbol{M}(\boldsymbol{x}, \lambda) - \boldsymbol{M}(\boldsymbol{x}, 0)$ in the first integral in (3.3) involves exponential functions with respect to the azimuthal angle ϕ, which may be evaluated by using regular numerical integration. In our implementation, we divide the interval $[0, 2\pi]$ into L divisions, and integrate over each division using the twelve- or twenty-point Gauss–Legendre quadrature. The maximum value of L in our calculations was 5.

Computations at high frequencies are prohibited by two pragmatic considerations. First, at high frequencies, the integrands in (3.3) exhibit pronounced fluctuations, requiring sophisticated but costly strategies of integration. Secondly, at high frequencies, the development of boundary layers requires boundary elements of small size, raising the cost of the computations to a prohibitive level.

The error due to the various approximations involved in the above procedure may be readily assessed following Higdon (1985). For particles with smooth boundaries, approximating the force distribution with a stepwise constant function introduces an error of $O(\delta^2)$, where δ is the length of a boundary element. Near corners, the error becomes of $O(\delta)$, but fortunately it affects the solution only locally. The error due to boundary discretization is a function of the geometry of the boundary elements. Straight segments yield error of $O(\delta^2)$ parabolas and circular arcs yield error of $O(\delta^4)$.

We performed computations using two types of boundary elements: straight segments and circular arcs. The two representations required comparable programming and computational effort. In both cases, the surface force was taken as a constant over each element, and thus, the overall error was of $O(\delta^2)$. For the arc representation, however, the magnitude of the error was reduced with respect to that for the straight segment representation, by as much as 10%.

To test our numerical procedure, as well as to verify the error analysis, we compared our numerical results with the analytical solution of Stokes for streaming flow past a sphere. The behaviour of the error was monitored by recording the real and imaginary part of the axial force on the sphere. Using straight segments gave a precise N^{-2} dependence for both the real and imaginary part of the force. Using circular arcs gave an N^{-2} dependence for the imaginary part of the force, but an N^{-3} dependence for the real part of the force. This seemingly paradoxical behaviour

can be understood by noting that using arcs eliminates the boundary discretization as a source of error, and also, that in the exact solution, the real part of the surface stress is a constant, whereas the imaginary part of it is a sinusoidal function.

The computations reported in the next section were performed on the CRAY X-MP/48 computer at SDSC. The solution of the integral equation with 48 boundary elements required approximately 3 min of CPU time. The maximum number of elements used was $N = 64$. Evaluation of the velocity at a point in the flow domain required approximately 4 s of CPU time. All of the results presented in the next section are accurate, in a global sense, to less than 0.5%.

4. Results and discussion

In the preceding sections we cast the problem of linearized oscillatory flow in integral form, and established a numerical procedure for treating axisymmetric motion. Our present goal is to probe into the physics of the flow by studying selected problems.

As we stated in the introduction, our major objective will be to assess the effect of the particle shape on the structure of the flow. We seek to accomplish this by selecting a reference problem, that is flow past a sphere, and by considering the change in the flow as the particle shape deviates from the reference state. We consider two classes of shapes: prolate and oblate spheroids, and particles in the form of dumbbells and biconcave disks. The former are chosen for their theoretical significance reflected in numerous previous investigations. The later are representative of particles with partially concave boundaries that are expected to exhibit distinct kinematical features.

4.1. *The sphere*

We prepare the grounds for our numerical results by discussing flow past a sphere, for which an analytical solution is available (Stokes 1851). To gain some physical insight into the structure of the flow, we present a sequence of instantaneous patterns for $|\lambda| = 1$ (figure 2). In the beginning of a cycle, $\omega t = 0$, when the outer flow has maximum strength towards the positive x-axis, all of the streamlines are smooth, conforming with the curvature of the sphere (figure 2*a*). As the flow decelerates, viscous forces near the surface of the sphere cause the fluid to reverse direction; at the critical time $\omega t = 0.375\pi$, a thin region of recirculating flow, having the form of an elongated eddy that is attached to the sphere, emerges. At later times, the developed eddy grows, its centre moving away from the sphere (figure 2*b*). Right in the middle of a cycle, $\omega t = 0.50\pi$, as the outer flow vanishes, the eddy attains very large dimensions, but then, as the flow reverses direction, it shrinks and disappears (figure 2*c*, *d*). Soon after that, during the accelerating flow period, the streamlines straighten out throughout the flow. We may describe this sequence of events as generation, expansion, and disappearance of an unsteady viscous eddy from a curved boundary. Increasing the frequency of the flow changes the structure, the lifetime, and the travel distance of an eddy, but leaves the qualitative features of the evolution unaffected.

To obtain further insights into the structure of the flow, it is helpful to consider the distribution of shear stress on the surface of the sphere, given by

$$\sigma_{\rm sh} = \tfrac{3}{2}(1+\delta-{\rm i}\delta)\,\sigma. \tag{4.1}$$

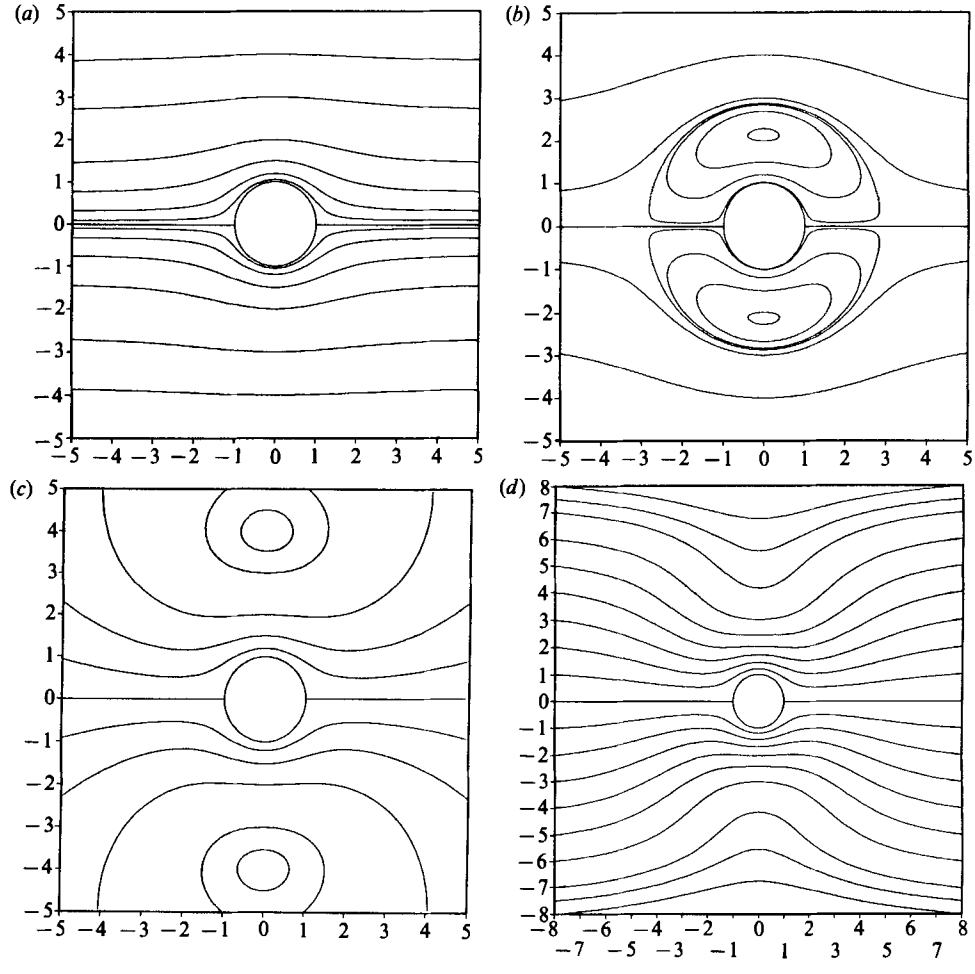

FIGURE 2. Instantaneous streamline patterns for flow past a sphere with $|\lambda| = 1.0$, at (*a*) $\omega t = 0$; (*b*) $\omega t = 0.45$; (*c*) $\omega t = 0.50$; (*d*) $\omega t = 0.51$. Note reduced scale in the last panel.

We note that the functional form of this distribution, linear in σ, is independent of the frequency of the motion. Furthermore, the phase of the distribution, $\phi = -\arctan(\delta/(\delta+1))$ is constant along the surface of the sphere. This suggests that the velocity in the vicinity of the sphere reverses direction at the same instant during each cycle of the motion, precluding the onset of stagnation points on the surface of the sphere. We shall see below that this is a unique feature of the spherical geometry.

The effect of the frequency $|\lambda|$ on the structure of the flow may be quantified by considering the velocity profile along the mid-plane of the sphere, at $x = 0, \sigma > a$ (figure 3*b*, *e*). Considering the magnitude of the velocity (figure 3*b*) we observe a smooth transition from the steady Stokes to the potential flow limit. The presence of a viscous boundary layer at $|\lambda| = 10$ becomes evident by comparing the velocity profile to the one for potential flow. Turning to the phase of the velocity (figure 3*e*), we see that at vanishingly small frequencies it is equal to zero throughout the flow. At small but finite frequencies it is negative, whereas at higher frequencies it may become positive. Recalling that the phase of oscillatory flow over a flat plate is

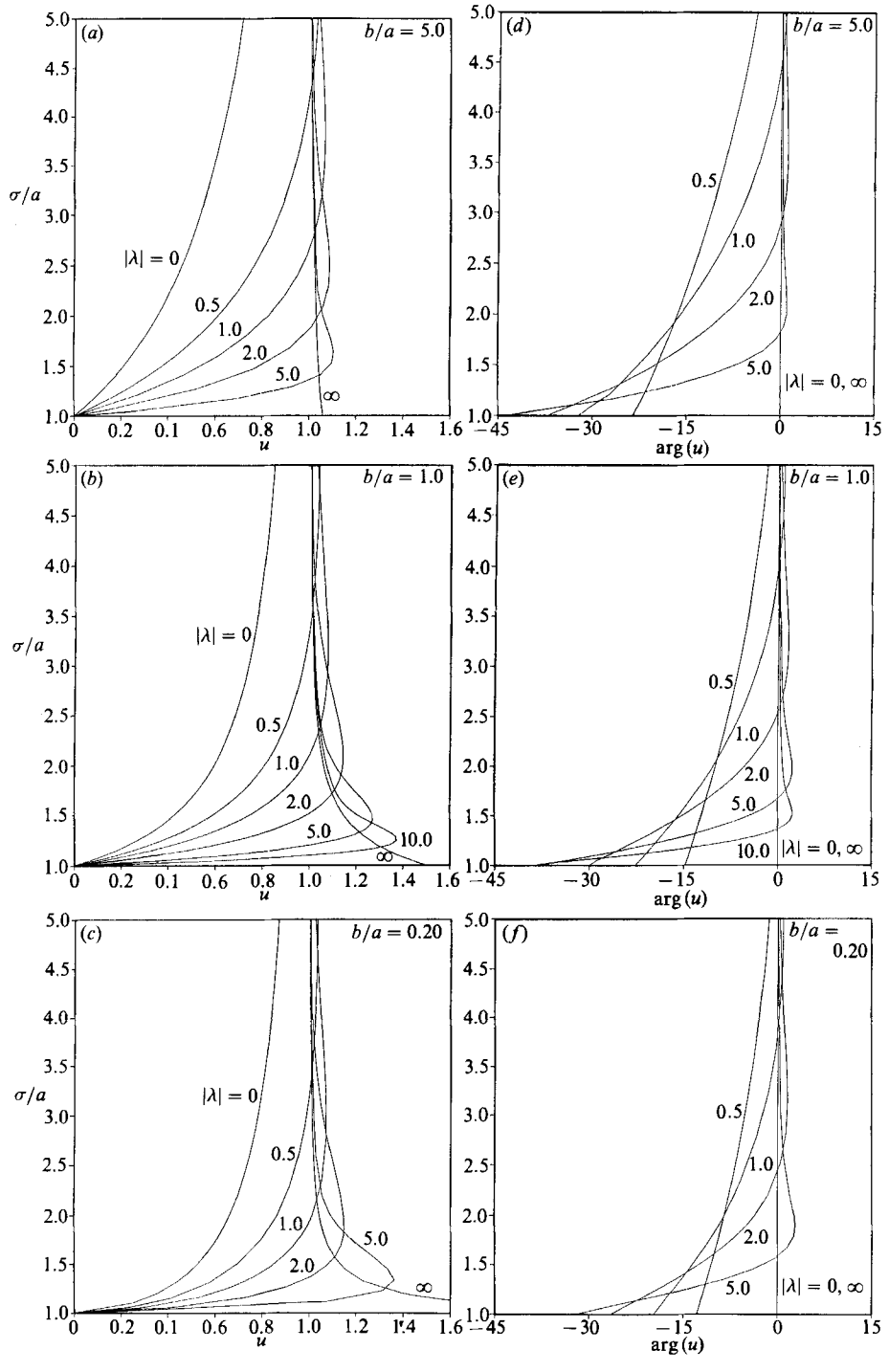

FIGURE 3. Velocity profiles along the particle midplane $x = 0$ for a prolate (a, d), a sphere (b, e), and an oblate spheroid (c, f). Panels (a, b, c) show the magnitude, and panels (d, e, f) the phase of the velocity; b/a is the aspect ratio of the spheroid.

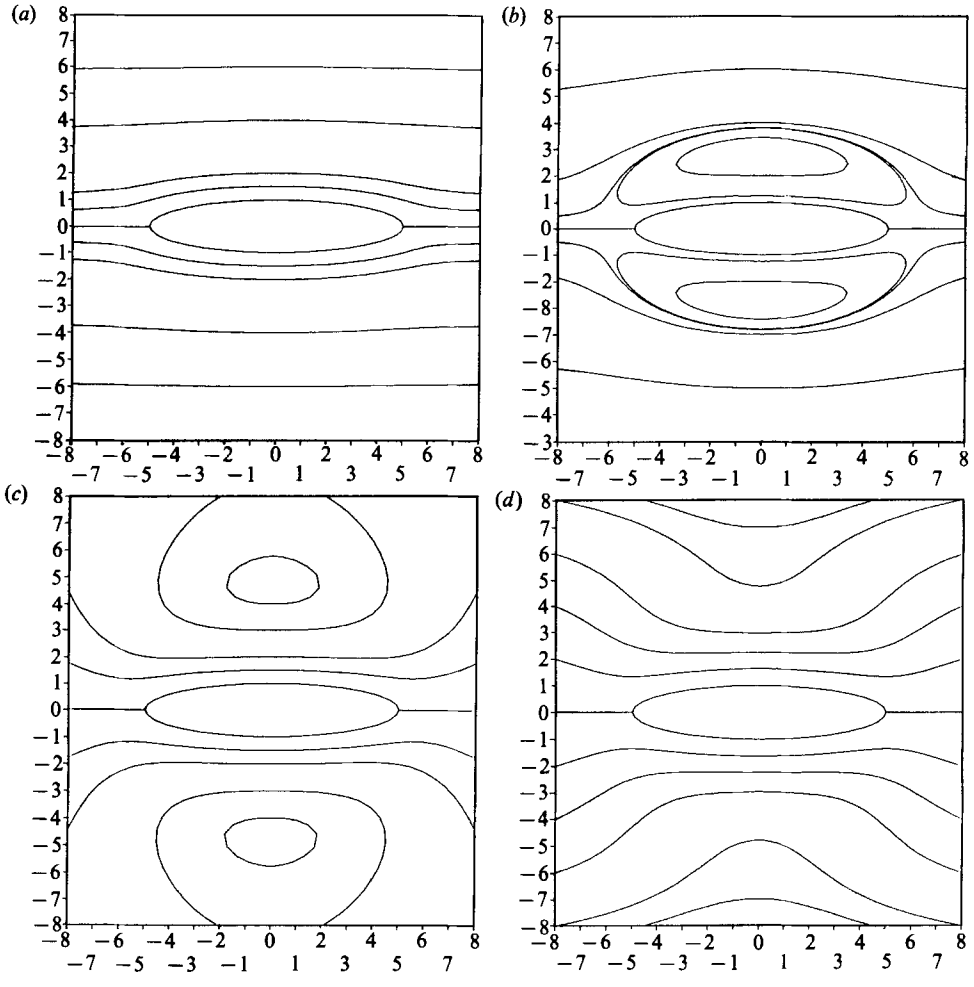

FIGURE 4. Instantaneous streamline patterns for flow past a prolate spheroid of $b/a = 5.0$, with $|\lambda| = 1.0$, at $\omega t = 0$; (*b*) $\omega t = 0.45$; (*c*) $\omega t = 0.50$; (*d*) $\omega t = 0.51$.

always negative, suggests that positive phase is attributed exclusively to the boundary curvature. As the frequency is increased, the phase of the velocity at a particular point decreases, reaches a negative minimum, and then it increases back to zero. The relationship between the phase and the frequency is not unique, and thus, one may not be deduced from the other. At very high frequencies, the phase at points far from the sphere tends to zero, whereas the phase at points very close to the surface of the sphere tends to $-45°$. This behaviour is consistent with boundary-layer theory (Batchelor 1967).

4.2. *Spheroids*

We begin our numerical investigation by considering streaming axial flow past prolate and oblate spheroids. We discuss our results with respect to the frequency parameter $|\lambda|$, defined by $\lambda^2 = -i\omega a^2/v$, where a is the axis of the spheroid perpendicular to the flow. The aspect ratio of the spheroid is equal to b/a, where b is the axis of the spheroid in the direction of the flow.

In figures 4 and 5 we present two sequences of instantaneous streamline patterns

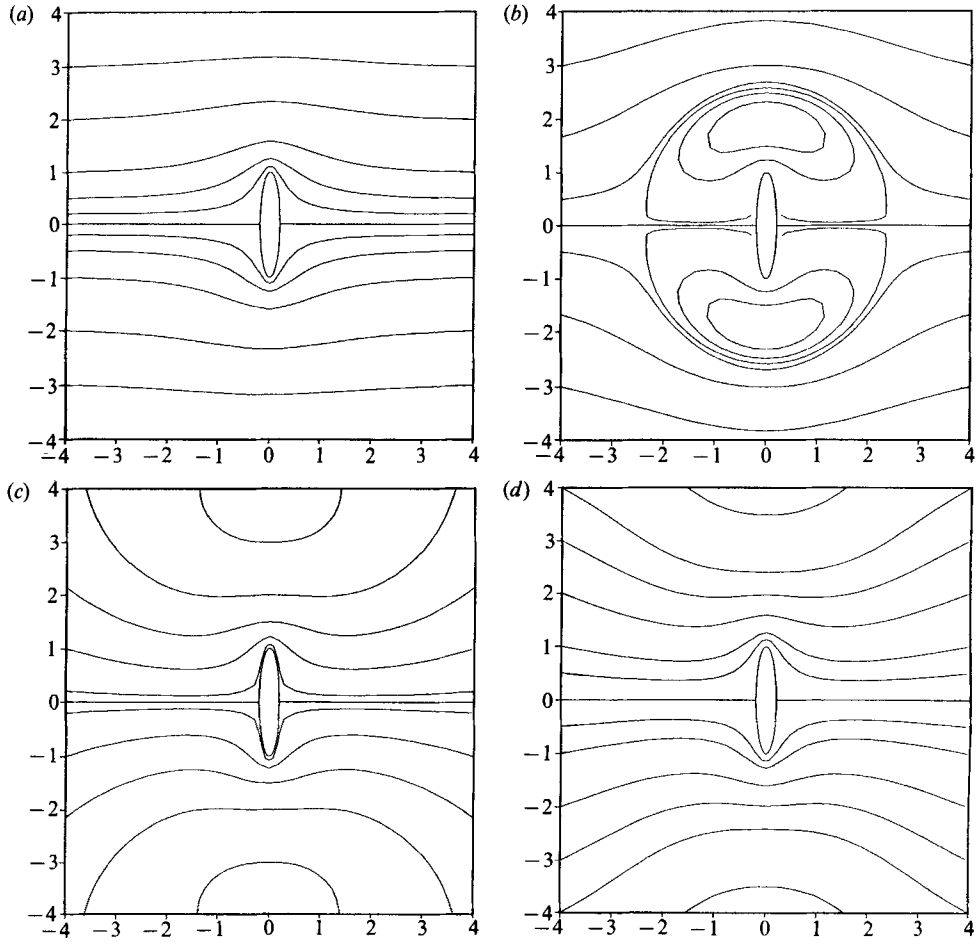

FIGURE 5. Instantaneous streamline patterns for flow past an oblate spheroid of $b/a = 0.20$, with $|\lambda| = 1.0$, at (*a*) $\omega t = 0$; (*b*) $\omega t = 0.45$; (*c*) $\omega t = 0.50$; (*d*) $\omega t = 0.51$.

for a prolate and an oblate spheroid of aspect ratio $b/a = 5.0$ and 0.2 respectively, and for $|\lambda| = 1.0$. Overall, we observe that the main features of the evolution are similar to those for the sphere: in all cases we obtain generation, expansion, and final disappearance of a viscous eddy. We note however that the shape of the dividing streamline enclosing an eddy conforms with the particle shape (figure 4*b*, 5*b*). More importantly, as we shall see below, the precise mechanism of eddy formation is dependent on the particle shape in a subtle manner.

We now address the flow in a more quantitative manner by considering the distribution of shear stress on the surface of the spheroids. It is important to note that the shear stress provides useful information not only on the structure of the flow, but also on the rate of simultaneous convective processes at high Péclet numbers (Higdon 1985). Indeed, in cases of material dissolution or deposition, the magnitude of the shear stress determines the location and direction of emerging protrusions or cavities.

We saw that the shear stress distribution on the sphere is a sinusoidal function with constant phase, at all frequencies. In figures 6 and 7 we present characteristic results for spheroids with $b/a = 5.0$ and 0.2. For clarity of illustration, in figure

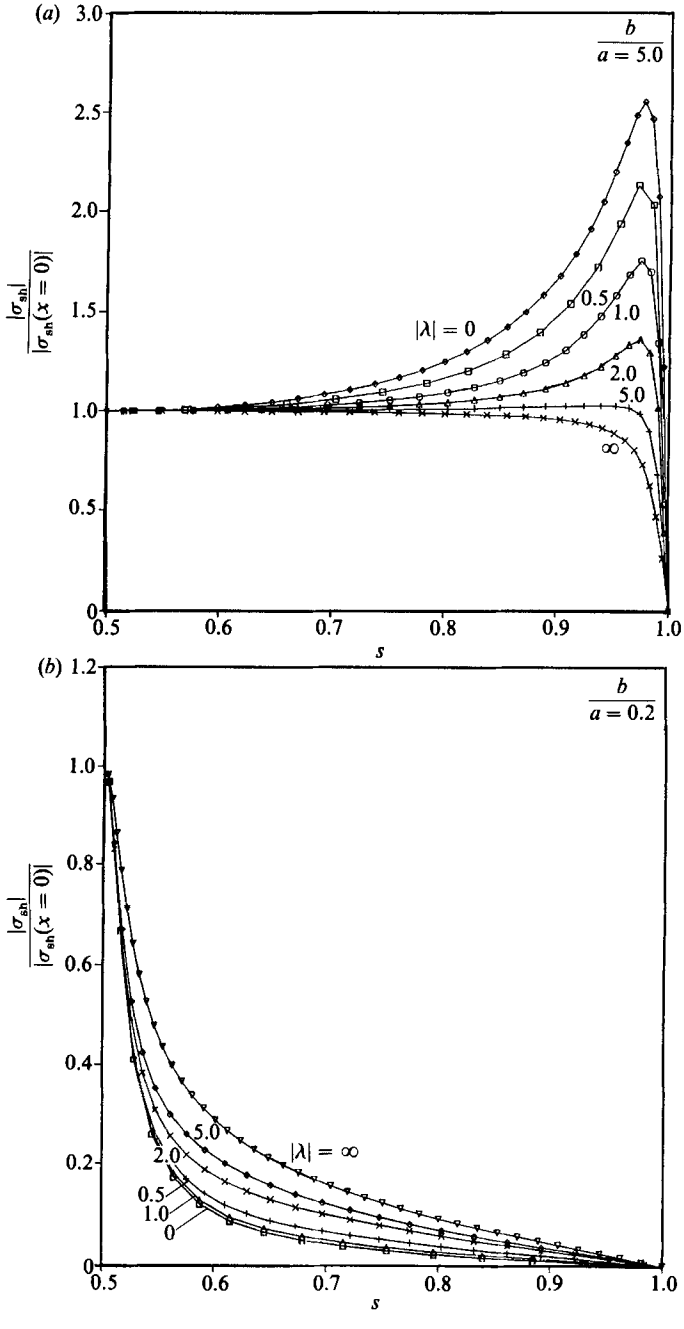

FIGURE 6. The magnitude of the shear stress along the surface of (*a*) a prolate and (*b*) an oblate spheroid for different frequencies; $s = 0.50$ corresponds to the midplane $x = 0$.

6(*a*, *b*) we have reduced the magnitude of the shear stress by that at the midplane of the spheroid (in absolute terms, the magnitude of the shear stress increases at an almost linear rate as $|\lambda|$ is increased). Considering figure 6(*a*, *b*), we observe a family of curves that are bounded by the one for steady Stokes flow and the one for potential flow (which is proportional to the tangential velocity along the surface of the

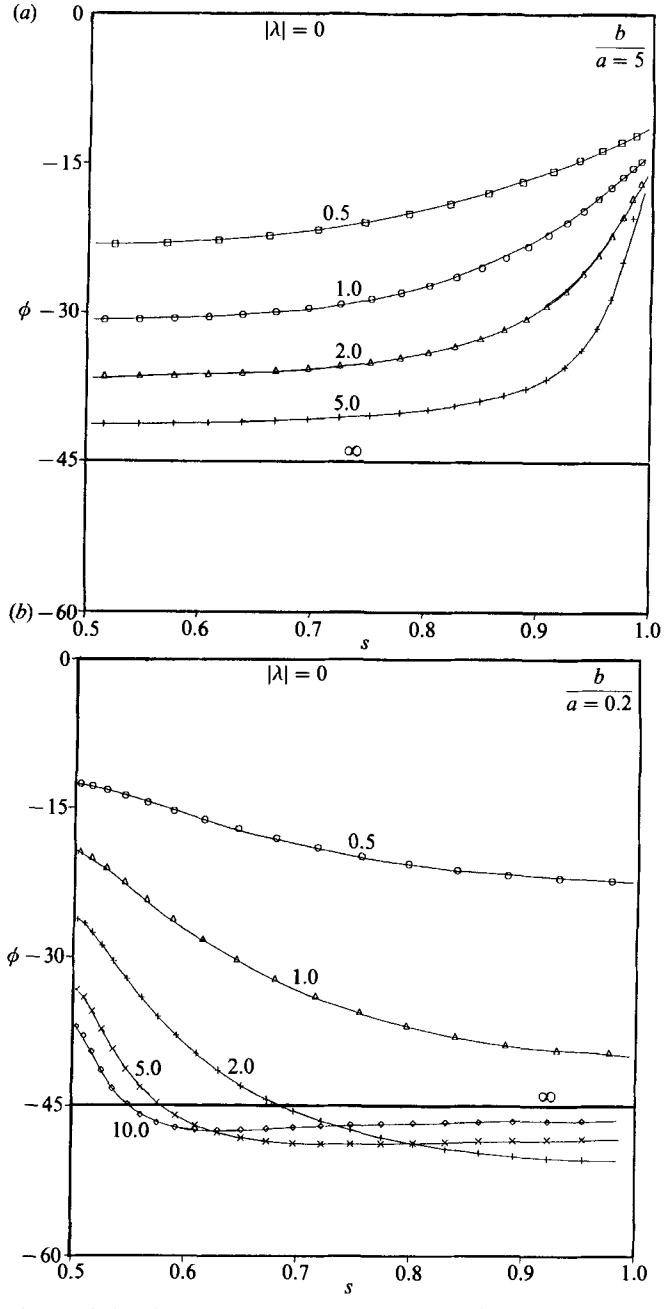

FIGURE 7. The phase of the shear stress (in degrees) along the surface of (*a*) a prolate and (*b*) an oblate spheroid.

spheroid in streaming potential flow, Lamb 1932, p. 141). For the sphere, these two extreme distributions coincide, but for spheroids they show quite distinct behaviour. For the prolate shape (figure 6*a*) there exists a maximum in each distribution; for steady flow this occurs near the tip of the spheroid, whereas for high-frequency flow it occurs at the midplane of the spheroid. In contrast, for the oblate shape (figure 6*b*) the maximum stress always occurs at the midplane of the spheroid. The shear stress

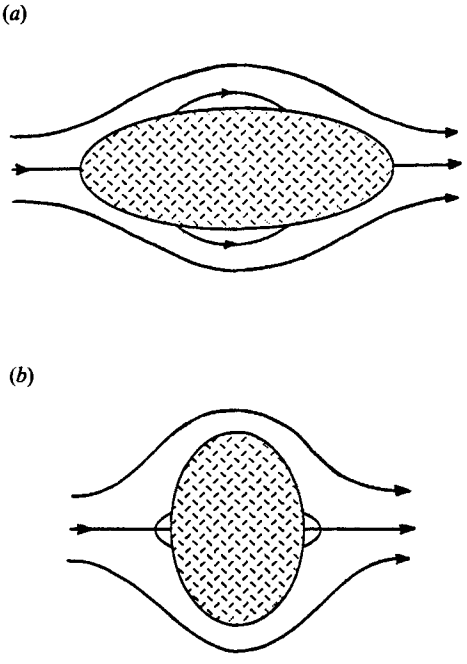

FIGURE 8. Schematic illustration of the motion of the stagnation points on the surface of (*a*) a prolate and (*b*) an oblate spheroid.

distribution becomes steeper around the maximum as the frequency is increased. In view of the above comments on the significance of the shear stress on convective processes, we conclude that the frequency of the flow is an important parameter in applications involving heat and mass transport.

We now examine the distribution of the phase of the shear stress $\phi(s)$, shown in figure 7 (*a*, *b*). At very low frequencies $\phi(s)$ vanishes, whereas at very high frequencies it tends to $-45°$, in accordance with boundary-layer theory (Batchelor 1967). For prolate spheroids $\phi(s)$ increases in a monotonic fashion from the centre to the tip of the particle. For oblate spheroids the inverse is true. We now recall that vanishing of the shear stress signals the appearance of a stagnation point, and thus, the presence of a viscous eddy attached to the particle. The shear stress vanishes when the real part of $\exp(\mathrm{i}(\phi-\omega t))$ becomes equal to zero, or equivalently, when $\omega t = \frac{1}{2}\pi - \phi + n\pi$, where n is an integer. We thus conclude that for prolate spheroids, a stagnation point appears at the particle midplane during the deceleration period ($0 < \omega t < \frac{1}{2}\pi$). It then starts travelling towards the tip of the spheroid, as shown in a schematic manner in figure 8(*a*). Finally, it detaches from the surface of the spheroid and moves along the x-axis into the flow. Further evolution is similar to that for the sphere. The travel speed of the stagnation point while on the surface of the particle is equal to $\mathrm{d}s/\mathrm{d}t = \omega(\mathrm{d}\phi/\mathrm{d}s)^{-1}$, whereas its total travel time is equal to $\Delta\phi/\omega$; $\Delta\phi$ is the total variation of the phase on the surface of the particle. For oblate spheroids, the stagnation point is born on the x-axis, it travels towards the particle midplane ($x = 0$), and merges with its symmetric counterpart to yield a closed recirculation region (figure 8*b*). Further evolution is similar to that for the prolate spheroid or for the sphere. Unfortunately, an accurate computation of streamline patterns showing the motion of stagnation points could not be achieved, restricting

us to the schematic illustrations of figure 8. In a more general context, the above results indicate that viscous eddies are generated at regions of low curvature during flow deceleration. Then, they expand and move away from their place of birth and into the flow. They shrink and disappear during the accelerating flow period.

It is of interest to consider velocity profiles along the particle midplane (figure 3*a*, *c*, *d*, *f*). Overall, these appear quite similar to those for the sphere, shown in figure 3(*b*, *e*). Cursory inspection though reveals certain interesting, subtle variations. First, one may observe that for prolate spheroids, the maximum attained velocity may exceed that for potential flow, figure 3(*a*). Secondly, for fixed frequency, the magnitude of the velocity at a particular point in the flow increases as the particle becomes more oblate. Furthermore, for fixed frequency, the phase of the velocity at a particular point decreases as the spheroid becomes more prolate. This implies that the flow has stronger viscous characteristics, attributed to the increased local boundary curvature. Prolate spheroids reach the boundary-layer flow regime at lower frequencies than oblate spheroids.

The total force on a spheroidal particle executing translational oscillations may be easily computed in our numerical procedure. Our results are in perfect agreement with those reported by Lawrence & Weinbaum (1988) and Pozrikidis (1988*b*).

4.3. *Dumbbells and biconcave disks*

In the second stage of our computations we consider axisymmetric particles whose contour is described by $r = a[1 + a_2 P_2(\theta)]$, where $r^2 = x^2 + \sigma^2$, θ is the polar angle, P_2 is the second-degree Legendre polynomial, a_2 is a scalar shape factor with values in the range $[-1, 2]$, and a is a characteristic lengthscale that we set equal to the maximum particle size in the σ direction. Positive a_2 defines prolate particles, whereas negative a_2 defines oblate particles. Values of a_2 below $-\frac{1}{4}$ or above $\frac{2}{7}$ yield particles with a partially concave shape, resembling dumbbells and biconcave disks respectively (figure 9). In our discussion we refer to the frequency parameter λ defined with respect to a, $\lambda^2 = -i\omega a^2/\nu$.

We begin by showing two characteristic instantaneous streamline patterns for a prolate and an oblate particle, $a_2 = 2.0$ and -0.80, and for $|\lambda| = 1.0$ (figure 9). As a new feature in the streamline pattern at $\omega t = 0$, we observe the presence of recirculating flow in the vicinity of the concave regions (figure 9*a*, *c*). During the decelerating flow period we observe the onset of the familiar unsteady free eddies enclosing the particle (figure 9*b*, *d*). We note in particular that these eddies coexist with wall corner eddies residing within the concave regions. The free eddies shrink and disappear during the accelerating flow period, but the wall corner eddies manage to survive throughout each cycle of the flow.

The precise behaviour of the wall corner eddies, and the associated motion of the wall stagnation points, becomes clear by considering the distribution of the magnitude and of the phase of the shear stress $\phi(s)$ on the particle surface (figures 10 and 11). In figure 10(*a*, *b*) we observe that the magnitude of the shear stress exhibits oscillatory decay within the concave regions. For steady flow, $|\lambda| = 0$, it vanishes at a number of points, indicating the presence of wall stagnation points that separate adjacent wall corner eddies. The precise structure of these steady eddies has been analysed by a number of authors including Dorrepaal *et al.* 1976*a*, *b*, Wakiya 1976 and Davis *et al.* 1976. As the frequency of the flow is increased, the magnitude of the shear stress becomes positive, shifting smoothly towards its potential flow limit. Turning to the phase of the shear stress $\phi(s)$, we notice that for steady flow it is discontinuous, undergoing a jump by 180° every time a stagnation point is crossed

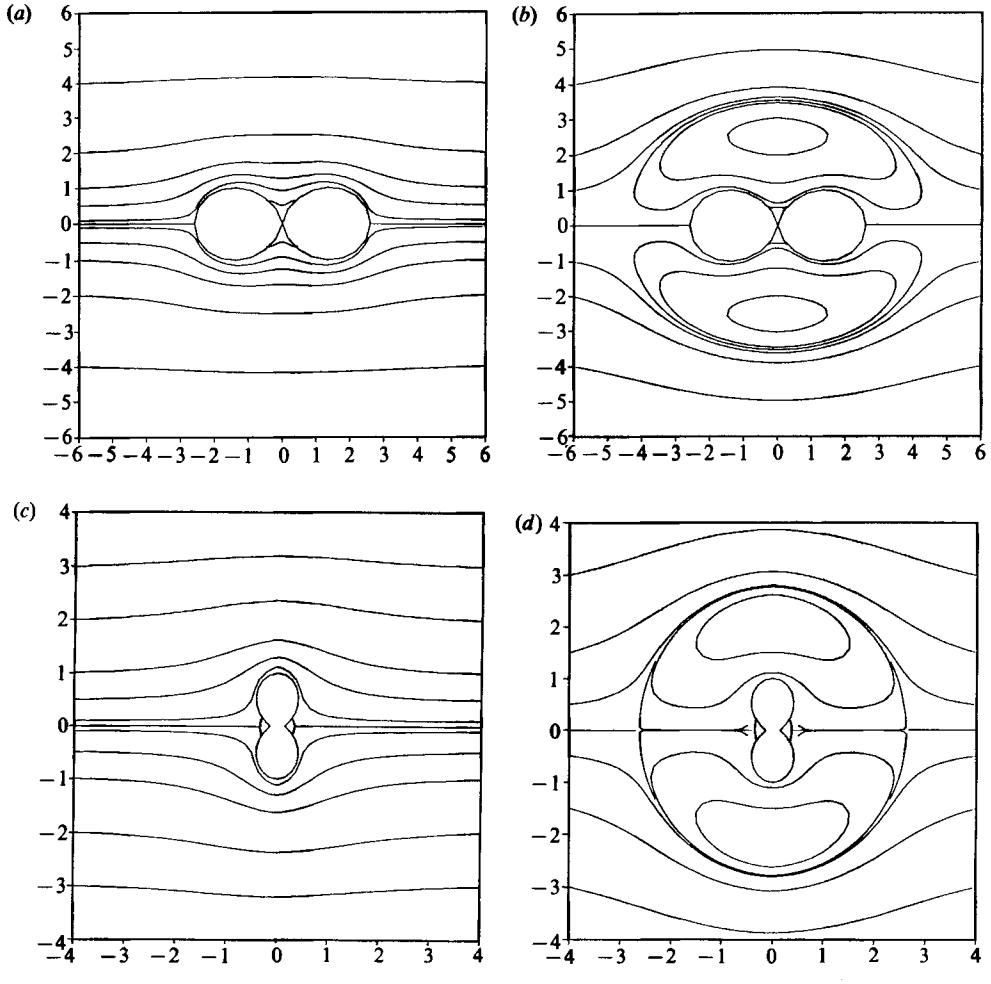

FIGURE 9. Instantaneous streamline patterns for flow past a dumbbell (a, b), and a biconcave disk (c, d) of $a_2 = 2$ and -0.80 respectively, with $|\lambda| = 1.0$, at (a) $\omega t = 0$; (b) $\omega t = 0.45$; (c) $\omega t = 0$; (d) $\omega t = 0.45$.

(figure 11 *a*, *b*). As the frequency is increased, $\phi(s)$ becomes continuous, with rapid variations within the concave regions (large $\mathrm{d}\phi/\mathrm{d}s$). At very high frequencies, $\phi(s)$ tends towards its asymptotic limit of $-45°$ dictated by boundary-layer theory.

To understand the behaviour of the wall eddies, we recall that the speed of a stagnation point on the particle surface is equal to $\mathrm{d}s/\mathrm{d}t = \omega(\mathrm{d}\phi/\mathrm{d}s)^{-1}$. This indicates that in the beginning of a cycle, the outermost stagnation point, located within the concave region, starts moving outwards very slowly, causing a correspondingly slow growth of the adjacent eddy. Then, it suddenly accelerates away from the concave region, travelling towards the tip or the midplane of the particle depending on whether the particle is prolate or oblate. This causes a sudden expansion of the accompanying eddy. Finally, it moves into the flow just as in the case of spheroids. The fact that the difference in $\phi(s)$ between two points on the particle surface may exceed 180° suggests that multiple wall eddies may coexist. When the outermost corner eddy starts expanding, the first eddy underneath moves to take its place. This eddy awaits expansion in the next cycle of oscillation.

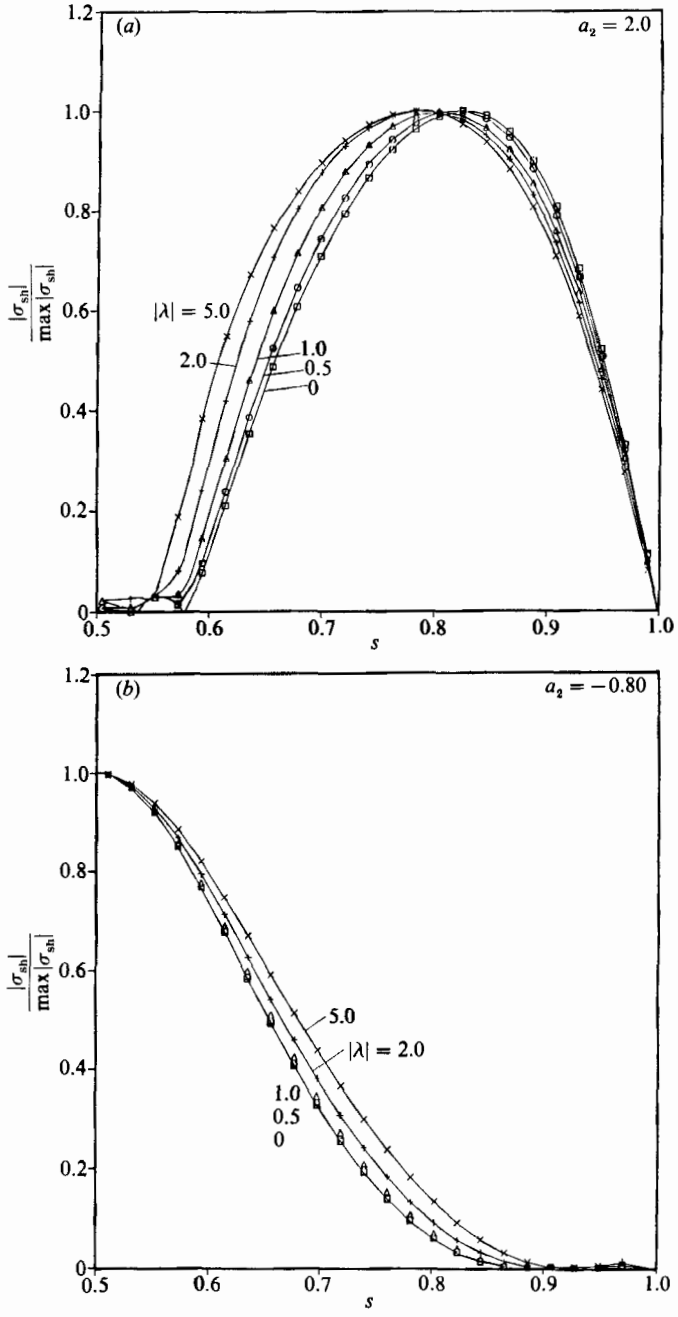

FIGURE 10. The magnitude of the shear stress along the surface of the dumbbell and the biconcave disk shown in figure 9; $s = 0.50$ corresponds to the particle midplane $x = 0$.

Thus, we see that in the case of a particle with concave boundaries, unsteady eddies may originate from the expansion of pre-existing corner eddies, rather than through the spontaneous appearance of stagnation points on the surface of the particle. For a particle with deep enough corrugations, corner eddies may coexist with free eddies evolving in the interior of the flow.

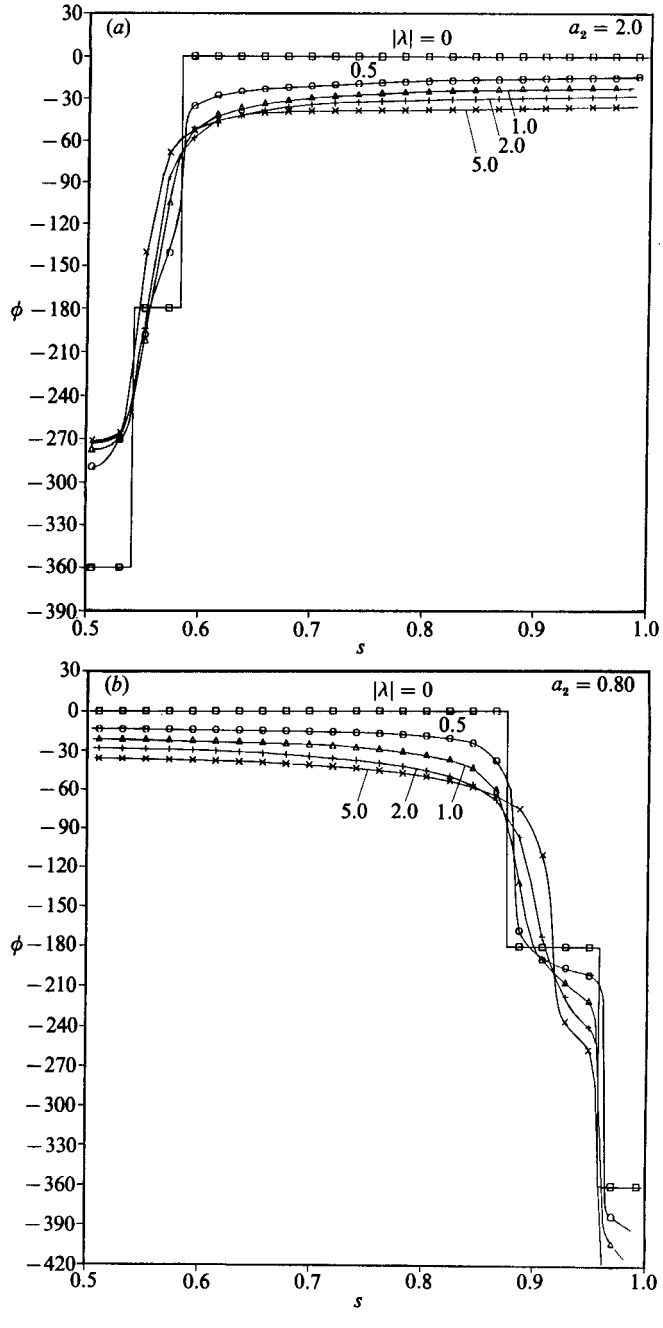

FIGURE 11. The phase of the shear stress along the surface of the dumbbell and the biconcave disk shown in figure 9.

Let us now consider the total force on dumbbells and biconcave disks executing translational oscillations (figure 12*a*, *b* and table 1). This is of interest in applications involving the motion of particle aggregates or red blood cells (having the shape of dumbbells and biconcave disks respectively), and provides us with the opportunity to discuss certain global characteristics of the flow. Due to the computational

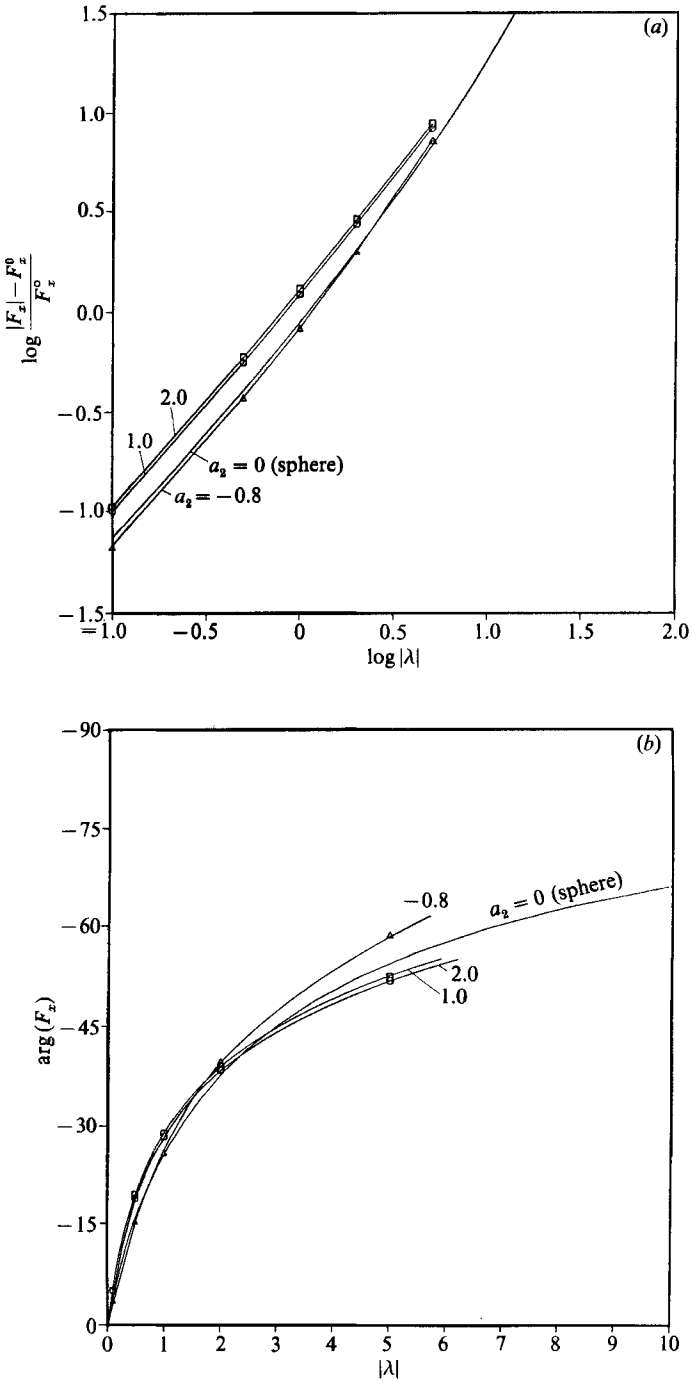

FIGURE 12. The magnitude (*a*), and phase (*b*) of the total force on dumbbells and biconcave disks in translational oscillation; F_x^0 stands for the steady Stokes resistance in axisymmetric motion.

$\lvert\lambda\rvert$	$a_2 = 2.00$		$a_2 = 1.00$		$a_2 = 0.80$	
0	26.762	0	25.347	0	17.303	0
0.1	29.570	−5.278	27.861	−5.025	18.460	−3.571
0.5	42.673	−19.425	39.549	−18.820	23.766	−5.325
1.0	61.421	−28.929	56.344	−28.370	31.745	−25.920
2.0	103.388	−38.895	94.164	−38.415	51.713	−39.588
5.0	260.796	−52.244	235.571	−51.689	141.855	−58.639

TABLE 1. The magnitude and phase (in degrees) of the axial force $\boldsymbol{F}/\mu va$ on dumbbells and biconcave disks in axial oscillation

difficulties discussed in §3, our results are limited to $|\lambda| < 5.0$. The magnitude of the force is shown in figure 12(*a*) on a log–log scale. At low frequencies, we observe a slope of unity in agreement with the asymptotic analysis of §2. At high frequencies we expect a slope of 2, owing to the dominant contribution of the resistance due to added mass. The transition from the low- to the high-frequency behaviour appears to be smooth despite the rather irregular particle shapes. At low frequencies, the force on prolate particles is higher than that on oblate particles, whereas at high frequencies the inverse is true. This is due to the fact that the viscous drag coefficient of prolate particles is pronounced owing to their increased surface area, but their added mass is reduced owing to their streamlined shape. The phase of the force is a measure of the relative importance of viscous and inertial forces, ranging between 0° and −90°, for quasi-steady and potential flow respectively. Accordingly, the phase of the axial force, shown in figure 12(*b*), indicates that oblate particles reach the potential flow regime at lower frequencies than prolate particles.

5. Closing remarks

Sobey (1980, §4.4) studied linearized oscillatory flow in two-dimensional furrowed channels using a finite difference method. He compared his results to those arising from the exact solution of full Navier–Stokes equations, and found good agreement for Reynolds numbers as high as 3.75. He also indicated that linearization is valid for arbitrary Reynolds number as long as the Strouhal number is of order one. His conclusions are in qualitative agreement with ours, and may be summarized as follows. Flow over curved boundaries reverses direction always in the decelerating time period. Depending on the frequency of the flow reversal may first occur over a concave or a convex boundary. The generated eddies expand around the time of zero mean flow. A free and a wall eddy may coexist in the vicinity of a curved boundary. Ralph (1986, §4) arrived at similar conclusions in his study of oscillatory flow in axisymmetric furrowed tubes. We may therefore conclude that the basic physical mechanisms of linearized oscillatory flow are independent of the type of geometry constricting the flow.

Acknowledgment is made to the donors of The Petroleum Research Fund, administered by the ACS, for partial support of this research. Thanks are due to the office of academic computing of UCSD for supporting this research.

Appendix A

The elements of the matrix $\boldsymbol{M}$ for axisymmetric, steady flow, are given as follows

$$M_{xx} = 2k\left(\frac{\sigma}{\sigma_0}\right)^{\frac{1}{2}}\left(F+\frac{\hat{x}^2}{r^2}E\right),$$

$$M_{x\sigma} = k\frac{\hat{x}}{(\sigma\sigma_0)^{\frac{1}{2}}}\left[F-(\sigma_0^2-\sigma^2+\hat{x}^2)\frac{E}{r^2}\right],$$

$$M_{\sigma x} = -k\frac{x}{\sigma_0}\left(\frac{\sigma}{\sigma_0}\right)^{\frac{1}{2}}\left[F+(\sigma_0^2-\sigma^2-\hat{x}^2)\frac{E}{r^2}\right],$$

$$M_{\sigma\sigma} = \frac{k}{\sigma\sigma_0}\left(\frac{\sigma}{\sigma_0}\right)^{\frac{1}{2}}\left[(2\hat{x}^2+\sigma_0^2+\sigma^2)F-\{2\hat{x}^4+3\hat{x}^2(\sigma_0^2+\sigma^2)^2\}\frac{E}{r^2}\right],$$

where F and E are the complete elliptic integrals of the first and second kind respectively, with argument

$$k^2 = \frac{4\sigma\sigma_0}{(x-x_0)^2+(\sigma+\sigma_0)^2}.$$

REFERENCES

Basset, A. B. 1888 *A Treatise on Hydrodynamics*, vol. 2. Cambridge: Deighton Bell.

Batchelor, G. K. 1967 *An Introduction to Fluid Dynamics*. Cambridge University Press.

Bentwich, M. & Miloh, T. 1978 The unsteady matched Stokes–Oseen solution for the flow past a sphere. *J. Fluid Mech.* **88**, 17–32.

Buchanan, J. 1891 The oscillations of a spheroid in a viscous fluid. *Proc. Lond. Math. Soc.* **22**, 181–214.

Chwang, A. T. & Wu, T. Y. 1975 Hydromechanics of low-Reynolds-number flow. Part 2. Singularity method for Stokes flows. *J. Fluid Mech.* **67**, 787–815.

Clift, R., Grace, J. R. & Weber, M. E. 1978 *Bubbles, Drops, and Particles*. Academic.

Dabros, T. 1985 A singularity method for calculating hydrodynamic forces and particle velocities in low-Reynolds-number flows. *J. Fluid Mech.* **156**, 1–21.

Davis, A. M. J., O'Neill, M. E., Dorrepaal, J. M. & Ranger, K. B. 1976 Separation from the surface of two equal spheres in Stokes flow. *J. Fluid Mech.* **77**, 625–644.

Dorrepaal, J. M., Majumdar, S. R., O'Neill, M. E. & Ranger, K. B. 1976*a* A closed torus in Stokes flow. *Q. J. Mech. Appl. Maths* **24**, 381–396.

Dorrepaal, J. M., O'Neill, M. E. & Ranger, K. B. 1976*b* Axisymmetric Stokes flow past a spherical cap. *J. Fluid Mech.* **75**, 273–286.

Ghaddar, N. K., Magen, M., Mikic, B. B. & Patera, A. T. 1986 Numerical investigation of incompressible flow in grooved channels. Part 2. Resonance and oscillatory heat-transfer enhancement. *J. Fluid Mech.* **168**, 541–567.

Gluckman, M. J., Pfeffer, R. & Weinbaum, S. 1971 A new technique for treating multiparticle slow viscous flow: axisymmetric flow past spheres and spheroids. *J. Fluid Mech.* **50**, 705–740.

Hall, P. 1974 Unsteady viscous flow in a pipe of slowly varying cross-section. *Fluid Mech.* **64**, 209–226.

Happel, J. & Brenner, H. 1983 *Low Reynolds Number Hydrodynamics*. Martinus Nijhoff.

Hasimoto, H. & Sano, O. 1980 Stokeslets and eddies in creeping flow. *Ann. Rev. Fluid Mech.* **12**, 335–363.

Higdon, J. J. L. 1985 Stokes flow in arbitrary two-dimensional domains: shear flow over ridges and cavities. *Fluid Mech.* **159**, 195–226.

HOWELLS, I. D. 1974 Drag due to the motion of a Newtonian fluid through a sparse random array of small fixed rigid objects. *J. Fluid Mech.* **64**, 449–475.

KANWAL, R. P. 1955 Rotatory and longitudinal oscillations of axi-symmetric bodies in a viscous fluid. *Q. J. Mech. Appl. Maths* **8**, 147–163.

KANWAL, R. P. 1964 Drag on an axially symmetric body vibrating slowly along its axis in a viscous fluid. *J. Fluid Mech.* **19**, 631–636.

KIM, S. 1986 Singularity solutions for ellipdoids in low-Reynolds-number flows: with applications to the calculation of hydrodynamic interactions in suspensions of ellipsoids. *Intl J. Multiphase Flow* **12**, 469–491.

KIM, S. & RUSSEL, W. B. 1985 The hydrodynamic interactions between two spheres in a Brinkman medium. *J. Fluid Mech.* **154**, 253–268.

LADYZHENSKAYA, O. A. 1969 *The Mathematical Theory of Viscous Incompressible Flow.* Gordon & Breach.

LAI, R. Y. S. & MOCKROS, L. F. 1972 The Stokes-flow drag on prolate and oblate spheroids during axial translatory accelerations. *J. Fluid Mech.* **52**, 1–15.

LAMB, H. 1932 *Hydrodynamics*, 6th edn. Cambridge University Press.

LAWRENCE, C. J. & WEINBAUM, S. 1986 The force on an axisymmetric body in linearized, time-dependent motion: a new memory term. *J. Fluid Mech.* **171**, 209–218.

LAWRENCE, C. J. & WEINBAUM, S. 1988 The unsteady force on a body at low Reynolds number; the axisymmetric motion of a spheroid. *J. Fluid Mech.* **189**, 463–489.

OSEEN, C. W. 1927 *Hydrodynamic.* Akademische verlagsgesellschaft M.B.H. Leipzig.

PADMANABHAN, N. & PEDLEY, T. J. 1987 Three-dimensional steady streaming in a uniform tube with an oscillating elliptical cross-section. *J. Fluid Mech.* **178**, 325–343.

PEDLEY, T. J. & STEPHANOFF, K. D. 1985 Flow along a channel with a time-dependent indentation in one wall: the generation of vorticity waves. *J. Fluid Mech.* **160**, 337–367.

PIENKOWSKA, I. 1984 Unsteady friction and mobility relations for Stokes flows. *Arch. Mech.* **36** (5–6), 749–769.

POZRIKIDIS, C. 1988*a* Flow of a liquid layer along a wavy wall. *J. Fluid Mech.* **188**, 275–300.

POZRIKIDIS, C. 1988*b* Linear oscillatory flow past particles and drops by the singularity method. *UCSD manuscript*, submitted for publication.

RALPH, M. E. 1986 Oscillatory flows in wavy-walled tubes. *J. Fluid Mech.* **168**, 515–540.

RILEY, N. 1967 Oscillatory viscous flows. Review and Extension. *J. Inst. Math. Applic.* **3**, 419–434.

SMITH, S. H. 1987 Unsteady Stokes' flow in two dimensions. *J. Engng Maths* **21**, 271–285.

SOBEY, I. J. 1980 On flow through furrowed channels. Part 1. Calculated flow patterns. *J. Fluid Mech.* **96**, 1–26.

SOBEY, I. J. 1982 Oscillatory flow at intermediate Reynolds number in asymmetric channels. *J. Fluid Mech.* **125**, 359–373.

SOBEY, I. J. 1983 The occurrence of separation in oscillatory flow. *J. Fluid Mech.* **134**, 247–257.

SOBEY, I. J. 1985*a* Observation of waves during oscillatory channel flow. *J. Fluid Mech.* **134**, 247–257.

SOBEY, I. J. 1985*b* Dispersion caused by separation during oscillatory flow through a furrowed channel. *Chem. Engng Sci.* **40**, 2129–2134.

STOKES, G. C. 1851 On the effect of fluids on the motion of pendulums. *Trans. Camb. Phil. Soc.* **9**, 8.

WAKIYA, S. 1976 Axisymmetric flow of a viscous fluid near the vertex of a body. *J. Fluid Mech.* **78**, 737–747.

WILLIAMS, W. E. 1966 A note on slow vibrations in a viscous fluid. *J. Fluid Mech.* **25**, 589–590.

YIH, C. C. 1979 *Fluid Mechanics.* West River Press.

YOUNGREN, G. K. & ACRIVOS, A. 1975 Stokes flow past a particle of arbitrary shape: a numerical method of solution. *J. Fluid Mech.* **69**, 377–403.